SYNTHESIS OF OPTIMAL CONTROLS AND NUMERICAL OPTIMIZATION FOR THE VIBRATION-BASED ENERGY HARVESTERS

Thuy T. T. Le[1], Binh D. Truong[2], Felix Jost[1], Cuong P. Le[2],
Einar Halvorsen[2] and Sebastian Sager[1]

Abstract. This work is devoted to demonstration of the mathematical analysis on maximizing the output power harvested from vibration energy harvester under a single sinusoid input with time-dependent amplitude or drive frequency. While most of recent works have investigated the use of mechanical nonlinearities to increase extractable power, or determining the optimal resistive load at steady-state operation of the transducers, real-time optimization problems have not been explored yet. In this paper, the stiffness and the electrical time constant are regarded as control subjects of linear two-port harvesters. The mathematical model is treated as an optimal control problem. Analysis of optimal controls is provided by means of *Pontryagin Maximum Principle*. Furthermore, making use of geometric methods of optimal control theory for this model, we are able to point out the *bang-bang* property of optimal controls. Finally, numerical results are illustrated to support our theoretical analysis and approach.

1. Introduction

Most of the energy used in electronics and sensor applications is supplied by batteries, which is very limited in operational lifetime. Especially, there are several environments where battery performance is restricted. Energy harvesting therefore becomes a key alternative for replacing battery roles in autonomous sensor networks [1, 2]. Due to the capability of providing electrical power harvested from mechanical vibration sources for electronic devices, energy harvesters are more and more concerned in recent researches. The energy storage cells such as rechargeable batteries or super-capacitors cannot intrinsically ensure an optimal power generation if directly connected to the rectifier output. A solution for the power optimization problem was proposed by Ottman et al. [3], using a dc-dc converter interleaved between the rectifier and the storage cells. They have shown that the optimal power point can be tracked by controlling the converter input average resistance. The power of a vibration-based generator strongly depends on the load. The power is maximized for matching load resistances, whose values are determined by the transducer figure of merit, external acceleration and vibration frequency [4]. A detailed discussion of optimizing power generated by a velocity damped resonant generator (VDRG), taking into account both of mechanical damping and electrical damping, is reported by Mitcheson et al. [5]. In summary,

Date: May 2, 2022.
Key words and phrases. two-port model, power optimization, vibration-based energy harvesters, Geometric Methods, Pontryagin Maximum Principle, switching function.

for unconstrained displacement or small forcing levels, and significant mechanical damping, the harvested power can be maximized by designing the electrical damping equal to the mechanical damping while the drive frequency is kept fix at resonant frequency. A bound on the output power of vibration energy harvesters when the proof mass is subject to parasitic, linear mechanical damping is determined on closed-form [6]. Halvorsen et at. proved that the optimal VDRG performance for a single sinusoid forcing coincides with the bound when the displacement is unconstrained. The same methodology is used to find the upper bound as a function of input vibration parameters with two more additional study cases, double sinusoid input and frequency-swept sinusoid input [7]. An analytical expression of the optimal load and stiffness of a linear two-port harvester driven by harmonic force under displacement-constrained operation was obtained in [8]. With the same perspectives, the optimum gap and load of the micro electret generator are also proved to be dependent on the proof mass displacement amplitude versus its limit [9].

However, research work mentioned above only examines the energy balance of the harvesting systems in steady state, which allows us to neglect the kinetic energy of the proof mass and the potential energy stored in the transducers. If the external driving force contains an amplitude that is varying over time, the complex conjugate matching method no longer works. Such situations will be investigated in this paper. From mathematical point of view, the linear two-port model consists of a strongly stiff system of ordinary differential equations (ODEs) due to the high frequency of the displacement. This causes difficulties in solving the problem numerically. Therefore, obtaining the approximate optimal power is a demanding task. The question of which values the stiffness and the electrical time constant should take in order to obtain maximized output power is studied analytically by classical methods in control theory, namely Pontryagin Maximum Principle and geometric methods of optimal control theory, see for instance [10,11]. Some applications of these methods for investigating optimization problems in medicine can be mentioned, such as antiangiogenic therapy in cancer treatment [12], the optimal delivery of combination therapy for tumors [13], a multi-input optimal control problem for combinations of cancer chemotherapy with immunotherapy in form of a boost to the immune system [14], or in optimum experimental design problems [15]. Their applications in ecomonics can be found in [16,17].

The structure of this paper is as follows. First, the linear two-port model is introduced. Then the analysis of optimal controls for this model is presented. We finally end up with solving the power optimization problems numerically under different settings with and without constraints, together with discussion to show how the numerical results fit our theoretical analysis and how much the output power can be improved by our approach.

2. Mathematical model

An example of a real electromechanical system is an overlap varying capacitance structure. The basic configuration of such an electrostatic energy harvester is shown in Figure 1. The design consists of the proof mass suspended in four linear springs with folded-beam. The transducers are operated by an external bias voltage connected to the movable mass. The

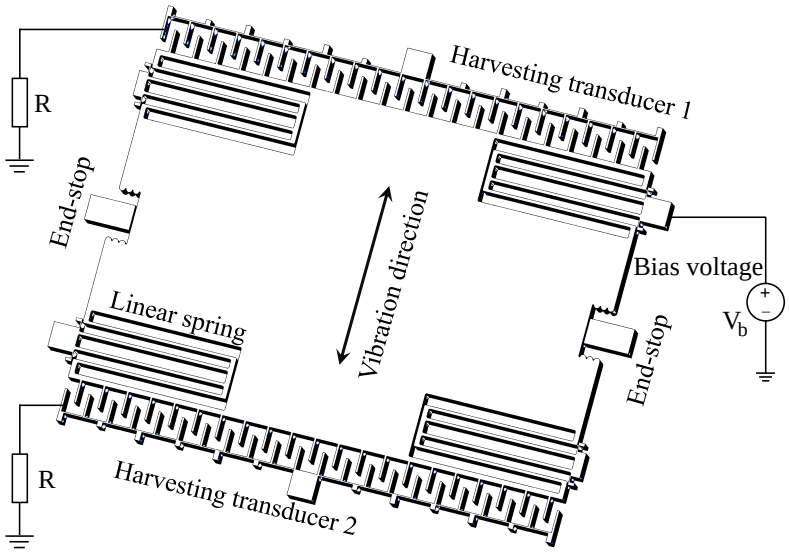

FIGURE 1. An electrostatic in-plane overlap varying energy harvester, an example of an electromechanical transducer.

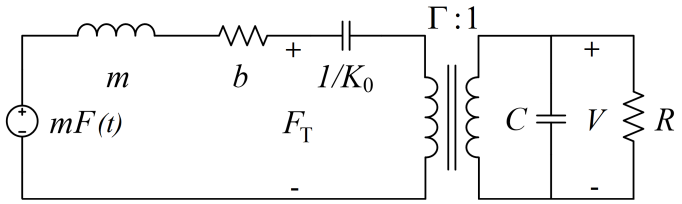

FIGURE 2. Electrical equivalent circuit of the linear two-port model.

output power is harvested by conversion from mechanical to electrical energy using capacitive transduction. The fixed electrodes are connected directly to external loads. Due to the restricted dimensions of the practical device, the mechanical end-stops are used to limit the proof mass motion and avoid beam fracture.

Transducers with three common mechanisms, i.e. piezoelectric, electrostatic and electromagnetic conversions, can be described by the linear two-port model with a single degree of freedom. The harvester is now no longer represented by complex differential equations and boundary conditions, but by a lumped-element circuit [18]. The elements are representatives of the transducer properties such as mass, stiffness, parasitic damping and variable capacitance. Equivalent circuits are widely used nowadays along with powerful mathematical techniques and network analysis programs, for instance LT-Spice (Simulation Program with Integrated Circuit Emphasis). Typically, an electrostatic energy generator can be modeled as a kinetic harvester with a generic transducer force F_{T} acting on the proof mass. The linear two-port equations for such a harvesting system are expressed as in [8]

$$F_{\mathrm{T}}(t) = Kx(t) + \frac{\Gamma}{C}q(t),\ V(t) = \frac{\Gamma}{C}x(t) + \frac{1}{C}q(t) \tag{2.1}$$

where K is the open-circuit stiffness, $x(t)$ is the displacement, $q(t)$ is the charge on the electrode, C represents the variable capacitor, Γ is the transduction factor and $V(t)$ is the voltage across the electrical port. Figure 2 depicts the equivalent circuit of the electrostatic generator, whereas the inertial mass m is subject to external forcing function $F(t)$ and the parasitic damping b. A load resistance R is connected directly to the electrical terminal. The short circuit stiffness K_0 is related to the open-circuit stiffness K by $K_0 = (1-k^2)K$, where the coupling factor is given by $k^2 = \frac{\Gamma^2}{KC}$.

Considering the open-circuit stiffness and the load resistance as *time-dependent functions*, the power optimization problem on a fixed time horizon $[t_0, t_\mathrm{f}]$ is formulated as follows

$$\max_{x(t),V(t),R(t),K(t)} \left(\frac{1}{t_\mathrm{f}-t_0} \int_{t_0}^{t_\mathrm{f}} \frac{V(t)^2}{R(t)} \right)$$

subject to

$$\begin{aligned} m\ddot{x}(t) &= -\left(K(t) - \frac{\Gamma^2}{C}\right) x(t) - b\dot{x}(t) - V(t)\Gamma + mF(t), \\ \dot{V}(t) &= \frac{\Gamma}{C}\dot{x}(t) - \frac{1}{R(t)C}V(t), \\ K(t) &\in [\underline{K}, \overline{K}],\ R(t) \in [\underline{R}, \overline{R}], \\ (x(t_0), y(t_0), V(t_0)) &= (x_0, y_0, V_0) \end{aligned} \tag{2.2}$$

where $0 \le t_0 < t_f < +\infty$, $\underline{K} > \frac{\Gamma^2}{C} > 0$, $\underline{R} > 0$, $\overline{K}, \overline{R} < +\infty$ and either $F(t) = F_\mathrm{a}(t) = A_\mathrm{r} t g \cos(\omega t)$ or $F(t) = F_\mathrm{f}(t) = A_\mathrm{c} g \cos(\omega_0 t + \frac{1}{2}\omega_\mathrm{r} t^2)$ with ω is the drive angular frequency, g is the gravitational acceleration, $A_\mathrm{r} = \frac{\Delta A}{\Delta t} = \frac{A_\mathrm{f} - A_0}{t_\mathrm{f} - t_0}$ has a unit of g s^{-1}, $\omega_\mathrm{r} = \frac{\Delta \omega}{\Delta t} = \frac{\omega_\mathrm{f} - \omega_0}{t_\mathrm{f} - t_0}$ has a unit of rad s^{-2}, where A_0 (ω_0) and A_f (ω_f) are acceleration amplitudes (angular frequencies) at t_0 (t_f) respectively. The value of A_c is kept fixed. The preceding problem containing a second-order ordinary differential equation (ODE) can be reduced to the one with merely first-order ODEs equivalently by introducing an auxiliary variable and denoting $u_1(t) = K(t)$, $u_2(t) = \frac{1}{R(t)}$ for convenience

$$\max_{x(t),y(t),V(t),u_1(t),u_2(t)} \left(\frac{1}{t_f - t_0} P(t_f) \right)$$

subject to

$$\begin{aligned} \dot{x}(t) &= y(t), \\ \dot{y}(t) &= -\frac{1}{m}\left(u_1 - \frac{\Gamma^2}{C}\right) x(t) - \frac{b}{m} y(t) - \frac{V(t)\Gamma}{m} + F(t), \\ \dot{V}(t) &= \frac{\Gamma}{C} y(t) - \frac{u_2}{C} V(t),\ \dot{P}(t) = V(t)^2 u_2(t), \\ u_1(t) &\in [\underline{u_1}, \overline{u_1}],\ u_2(t) \in [\underline{u_2}, \overline{u_2}] \\ (x(t_0), y(t_0), V(t_0), P(t_0)) &= (x_0, y_0, V_0, 0). \end{aligned} \tag{2.3}$$

3. Analysis of optimal controls

3.1. **Pontryagin Maximum Principle.** Let us start by introducing some terminologies used in this work. A control $u\colon [t_0, t_f] \to [\underline{u}, \overline{u}]$ only switching between the lower and upper bounds of the compact control set, i.e. $\underline{u}$ and $\overline{u}$, is called *bang-bang*, while it is called *singular* if u takes values in the interior of the control set. For the sake of shortness, we prefer to write x, y, V, P instead of $x(t), y(t), V(t), P(t)$ if there is no confusion and introduce $X = (x, y, V, P)^T$, $u = (u_1, u_2)^T$ and

$$f(X,t) = \left(y, \frac{\Gamma^2 x}{mC} - \frac{by}{m} - \frac{\Gamma V}{m} + F(t), \frac{\Gamma y}{C}, 0\right)^T,$$
$$g_1(X) = \left(0, -\frac{x}{m}, 0, 0\right)^T, \; g_2(X) = \left(0, 0, -\frac{V}{C}, V^2\right)^T,$$

then the system of ODEs in (2.3) becomes

$$\dot{X} = f(X,t) + g_1(X)u_1 + g_2(X)u_2 := R_d(X,t,u). \tag{3.1}$$

Let us first recall the first-order necessary conditions for optimality of controls u_1, u_2 given by the classical Pontryagin Maximum Principle (PMP) [10,11]. The PMP says that if $u_1^\star$, $u_2^\star$ are optimal controls with the corresponding optimal trajectories $(x^\star, y^\star, V^\star, P^\star)^T$ on the interval $[t_0, t_f]$, there exist a constant $\lambda_0 \geq 0$ and an absolutely continuous adjoint vector (a row vector) $\lambda(t)\colon [t_0, t_f] \to \mathbb{R}^4$ such that

(1) Nontriviality of the multipliers: $(\lambda_0, \lambda(t)) \neq 0$ for all $t \in [t_0, t_f]$,

(2) Adjoint equations: $\lambda(t)$ is the solution of the following adjoint equations

$$\begin{aligned}
\dot{\lambda}_1(t) &= -\lambda_2(t)\left(\frac{\Gamma^2}{Cm} - \frac{u_1^\star}{m}\right),\\
\dot{\lambda}_2(t) &= -\lambda_1(t) + \lambda_2(t)\frac{b}{m} - \lambda_3(t)\frac{\Gamma}{C},\\
\dot{\lambda}_3(t) &= \lambda_2(t)\frac{\Gamma}{m} + \lambda_3(t)\frac{u_2^\star}{C} - 2\lambda_4(t)u_2^\star V^\star,\\
\dot{\lambda}_4(t) &= 0,
\end{aligned} \tag{3.2}$$

together with the tranversality condition $\lambda(t_f) = (0, 0, 0, \lambda_0)$.

(3) Maximum condition: the optimal controls $u_1^\star$, $u_2^\star$ maximize the *Hamiltonian* H

$$H(X, \lambda, t, u) = < \lambda(t), f(X,t) + g_1(X)u_1 + g_2(X)u_2 >$$

along $(\lambda(t), x^\star, y^\star, V^\star, P^\star)$ over $[\underline{u_1}, \overline{u_1}]$ and $[\underline{u_2}, \overline{u_2}]$ respectively, in particular

$$H(X^\star, \lambda, t, u^\star) = \max_{u_1 \in U_1,\, u_2 \in U_2} < \lambda(t), f(X^\star, t) + g_1(X^\star)u_1 + g_2(X^\star)u_2 >,$$

where $U_1 = [\underline{u_1}, \overline{u_1}]$, $U_2 = [\underline{u_2}, \overline{u_2}]$.

Remark 3.1. *It is obvious that $\lambda_0 \neq 0$ (which implies $\lambda_0 > 0$) since otherwise the system (3.2) has a trivial solution and therefore the condition (1) of PMP is violated.*

3.2. **Synthesis of optimal controls via switching functions.** Let us rewrite the Hamiltonian as

$$H(X, \lambda, t, u) =< \lambda(t), f(X, t) > +\Phi_1(t)u_1 + \Phi_2(t)u_2,$$

where $\Phi_1(t) =< \lambda(t), g_1(X) >$, $\Phi_2(t) =< \lambda(t), g_2(X) >$. The structures of the optimal controls are determined by the properties of the switching functions $\Phi_1(t)$, $\Phi_2(t)$. As long as $\Phi_1(t)$, $\Phi_2(t)$ are not zero, then due to the maximum condition (3) of PMP above the optimal controls are given by

$$u_1^\star = \begin{cases} \underline{u_1} \text{ if } \Phi_1(t) < 0 \\ \overline{u_1} \text{ if } \Phi_1(t) > 0 \end{cases}, u_2^\star = \begin{cases} \underline{u_2} \text{ if } \Phi_2(t) < 0 \\ \overline{u_2} \text{ if } \Phi_2(t) > 0 \end{cases}.$$

The optimal controls cannot be determined by the maximum condition if $\Phi_1(t)$, $\Phi_2(t)$ are equal to zero. In this case, some information about the structures of optimal controls can be obtained by analyzing their derivatives up to an appropriate order of the switching functions, see [10, Chapter 2].

In general, the optimal controls are synthesized from potential candidates of optimality which are concatenations of bang-bang and singular types via the analysis of the zero sets of $\Phi_1(t)$, $\Phi_2(t)$

$$Z_1 = \{t \in [t_0, t_f] \colon \Phi_1(t) = 0\},$$
$$Z_2 = \{t \in [t_0, t_f] \colon \Phi_2(t) = 0\}.$$

Unfortunately, we have little knowledge about them, but from [10, Chapter 2] it follows that they are closed sets. The following proposition taken from [10, Chapter 2] is a very efficient and elegant tool from geometric control theory which allows the derivatives of switching functions to be expressed in compact forms.

Proposition 3.2 ([10, Chapter 2]). *Let γ be a continuously differentiable vector field and*

$$\Gamma(t) =< \lambda(t), \gamma(X(t)) > .$$

Then along a solution to (3.1) for controls u_1, u_2 and an adjoint solution to (3.2) the time derivative of $\Gamma(t)$ is given by

$$\dot{\Gamma}(t) =< \lambda(t), [f + g_1u_1 + g_2u_2, \gamma](X(t)) >$$

where $[a, b](X) = Db(X)a(X) - Da(X)b(X)$ denotes the Lie bracket of vector fields a, b and $Da(X)$, $Db(X)$ are matrices of partial derivatives of a, b along $X(t)$.

For more properties of the Lie brackets, we refer to e.g. [10, Chapter 2]. In what follows, we make use of Proposition 3.2 to study potential candidates of the controls for optimality.

3.3. **Analysis of optimal controls.** This section is devoted to studying the zero sets Z_1, Z_2 by analyzing the derivatives of $\Phi_1(t)$, $\Phi_2(t)$ with the help of Proposition 3.2. We will point out that Z_1, Z_2 are countable, i.e. $\Phi_1(t)$, $\Phi_2(t)$ have countable switchings. Therefore the potential candidates of the optimal controls u_1, u_2 for the problem (2.3) are bang-bang ones. We have

$$\Phi_1(t) =< \lambda(t), g_1(X) >= -\lambda_2(t)\frac{x}{m},$$
$$\Phi_2(t) =< \lambda(t), g_2(X) >= -\lambda_3(t)\frac{V}{C} + \lambda_4(t)V^2.$$

Owing to Proposition 3.2, it is easy to obtain the first derivatives of $\Phi_1(t)$ and $\Phi_2(t)$ as

$$\begin{aligned}\dot{\Phi}_1(t) &=< \lambda(t), [R_d(X,u,t), g_1(X)] > \\ &= \lambda_1(t)\frac{x}{m} - \lambda_2(t)\left(\frac{bx}{m^2} + \frac{y}{m}\right) + \lambda_3(t)\frac{\Gamma x}{Cm}, \\ \dot{\Phi}_2(t) &=< \lambda(t), [R_d(X,u,t), g_2(X)] > \\ &= -\lambda_2(t)\frac{\Gamma V}{Cm} - \lambda_3(t)\frac{\Gamma y}{C^2} + \lambda_4(t)\frac{2\Gamma V y}{C}.\end{aligned}$$

Obviously, if $\Phi_1(t) = 0$ and $\dot{\Phi}_1(t) \neq 0$ ($\Phi_2(t) = 0$ and $\dot{\Phi}_2(t) \neq 0$), u_1 (u_2) switches between $\underline{u_1}$ and $\overline{u_1}$ ($\underline{u_2}$ and $\overline{u_2}$). We are going to show that there exists no time interval on which both $\Phi_1(t)$ and all its derivatives of $\Phi_1(t)$ vanish, i.e. u_1 is a bang-bang control. Similarly, we will point out that u_2 is also a bang-bang control.

Remark 3.3. *There exists no time interval $(t_1, t_2) \subset [t_0, t_f]$ on which $V(t) = 0$ since otherwise the system of ODEs in (2.3) has no solution for any controls u_1, u_2.*

Proposition 3.4. *The switching function $\Phi_1(\cdot)$ has a finite number of switchings over $[t_0, t_f]$ and therefore the optimal control u_1 is of a bang-bang type.*

Proof. We are going to prove this proposition by assuming contradictorily that there exists $(t_1, t_2) \subset [t_0, t_f]$ on which $\Phi_1(t)$ and all its derivatives vanish. We have

$$\Phi_1(t) = -\lambda_2(t)\frac{x}{m} = 0,$$

which leads to either $\lambda_2(t) = 0$ or $x = 0$.

(i) if $\lambda_2(t) = 0$, then owing to (3.2) we have

$$\begin{aligned}\dot{\lambda}_1(t) &= 0, \\ \dot{\lambda}_2(t) &= -\lambda_1(t) - \lambda_3(t)\frac{\Gamma}{C}, \\ \dot{\lambda}_3(t) &= \lambda_3(t)\frac{u_2}{C} - \lambda_4(t)2u_2V, \\ \dot{\lambda}_4(t) &= 0.\end{aligned}$$

Since $\lambda_2(t) = 0$ on (t_1, t_2), $\dot{\lambda}_2(t) = 0$. Thus from the above system we derive $\lambda_1(t) = -\lambda_3(t)\frac{\Gamma}{C}$, therefore

$$\dot{\Phi}_1(t) = \lambda_1(t)\frac{x}{m} - \lambda_2(t)\left(\frac{bx}{m^2} + \frac{y}{m}\right) + \lambda_3(t)\frac{\Gamma x}{Cm} = 0.$$

By differentiating both sides of $\lambda_1(t) = -\lambda_3(t)\frac{\Gamma}{C}$ and taking into account $\dot{\lambda}_1(t) = 0$, we obtain $\dot{\lambda}_1(t) = -\dot{\lambda}_3(t)\frac{\Gamma}{C}$ which implies $\dot{\lambda}_3(t) = 0$ and $\lambda_3(t) = 2\lambda_4(t)CV$, thus $\dot{V} = 0$, i.e. $y = \frac{u_2}{\Gamma}V$ due to (2.3). Observe that $t_2 \neq t_f$ since otherwise, $(\lambda_0, \lambda(t)) = 0$

which violates the conditions of optimality and $t_1 \neq t_0$ due to (2.3) and Remark 3.3. On the other hand, we have

$$\Phi_2(t) =< \lambda(t), g_2(X) >= -\lambda_4(t)V^2 \neq 0$$

which means that u_2 is a bang-bang control. Thus $y = \frac{u_2}{\Gamma}V$ implies $\dot{y} = \frac{u_2}{\Gamma}\dot{V} = 0$. Owing to (2.3),

$$-\frac{1}{m}\left(u_1 - \frac{\Gamma^2}{C}\right)x - \left(b\frac{u_2}{\Gamma} + \Gamma\right)\frac{V}{m} + F(t) = 0. \tag{3.3}$$

By means of $\lambda_1(t) = -\lambda_3(t)\frac{\Gamma}{C}$, $\lambda_2(t) = 0$, $\lambda_3(t) = 2\lambda_4(t)CV$, $y = \frac{u_2}{\Gamma}V$ and (3.3), we obtain

$$\begin{aligned}
\ddot{\Phi}_1(t) =& < \lambda(t), [R_d(X,u,t), [R_d(X,u,t), g_1(X)]] > \\
=& \frac{\lambda_4(t)2V}{m}\left(-\Gamma\frac{bx+2my}{m} + \frac{\Gamma(bCx + mu_2x + 2Cmy)}{Cm} - \frac{\Gamma u_2 x}{C}\right) = 0, \\
\Phi_1^{(3)}(t) =& < \lambda(t), [R_d(X,u,t), [R_d(X,u,t), [R_d(X,u,t), g_1(X)]]] > \\
=& -\frac{2\Gamma\lambda_4(t)u_2x\,(\Gamma y - u_2V)}{C^2m} = 0
\end{aligned}$$

automatically and

$$\begin{aligned}
\Phi_1^{(4)}(t) =& < \lambda(t), [R_d(X,u,t), [R_d(X,u,t), [R_d(X,u,t), [R_d(X,u,t), g_1(X)]]]] > \\
=& \frac{2\Gamma\lambda_4(t)u_2\left(C\left(bu_2Vx - F(t)\Gamma mx + \Gamma^2Vx + \Gamma u_1x^2\right) - \Gamma^3x^2\right)}{C^3m^2} = 0
\end{aligned}$$

provided (3.3), i.e. the control may be a singular arc

$$u_1(t) = \frac{-\left(b\frac{u_2}{\Gamma} + \Gamma\right)V(t) + mF(t)}{x(t)} + \frac{\Gamma^2}{C} \tag{3.4}$$

since $x(t) \neq 0$ (otherwise, the system of ODEs in (2.3) has no solution for any u_1, u_2 under the conditions $\dot{y} = \dot{V} = 0$). Meanwhile,

$$\begin{aligned}
\Phi_1^{(5)}(t) =& < \lambda(t), [R_d(X,u,t), [R_d(X,u,t), [R_d(X,u,t), [R_d(X,u,t), [R_d(X,u,t), g_1(X)]]]]] > \\
=& -\frac{2\lambda_4(t)u_2^2V\left(V\left(bu_2 + \Gamma^2\right) - F(t)\Gamma m\right)}{C^2m^2} = \frac{2\lambda_4(t)u_2^2V\left(u_1 - \frac{\Gamma^2}{C}\right)x(t)}{\Gamma C^2m^2} \neq 0
\end{aligned}$$

due to (3.4). This means that there is no time interval on which $\Phi_1(t)$ and all its derivatives vanish, i.e. u_1 switches between $\underline{u_1}, \overline{u_1}$, or in other words u_1 is a bang-bang control.

(ii) if $x = 0$, $\lambda_2(t) \neq 0$, due to (2.3) we obtain also $y = 0$ and

$$\begin{cases} V = \frac{m}{\Gamma}F(t), \\ \dot{V} = \frac{-u_2}{C}V, \end{cases}$$

which implies $u_2 = \frac{-F(\dot{t})C}{F(t)}$ when $\{t : F(t) = 0\} \cap (t_1, t_2) = \emptyset$ (since $F(t)$ has finite zeros on $[t_0, t_f]$, it is always possible to take (t_1, t_2) such that the intersection is an empty set). While $\dot{\Phi}_2(t) = -\lambda_2(t)\frac{\Gamma V}{Cm} \neq 0$ on (t_1, t_2) due to Remark 3.3 which means that u_2 switches between $\underline{u_2}$ and $\overline{u_2}$ and this is a contradiction to $u_2 = \frac{-F(\dot{t})C}{F(t)}$.

Therefore $\Phi_1(t)$ and its derivatives cannot vanish on any time intervals $(t_1, t_2) \subset [t_0, t_f]$ which means that u_1 is only of a bang-bang type. □

Similarly, we drive the following proposition which determines the structure of u_2.

Proposition 3.5. *The switching function $\Phi_2(\cdot)$ has a finite number of switchings over $[t_0, t_f]$, i.e. the optimal control candidate u_2 is of a bang-bang type.*

Proof. Assume there exists $(t_1, t_2) \subset [t_0, t_f]$ such that $\Phi_2(t)$ and all derivatives vanish for every t in (t_1, t_2). Owing to $\Phi_2(t) = 0$ and $\dot{\Phi}_2(t) = 0$ we receive

$$\begin{aligned} \lambda_3(t) &= C\lambda_4(t)V, \\ \lambda_2(t) &= \lambda_4(t)ym. \end{aligned} \tag{3.5}$$

By plugging $\lambda_2(t) = \lambda_4(t)ym$, $\lambda_3(t) = C\lambda_4(t)V$ into (3.2), we receive

$$\begin{cases} \dot{\lambda}_1(t) = -\lambda_4(t)y\left(\frac{\Gamma^2}{C} - u_1\right), & \lambda_1(t_f) = 0 \\ \dot{\lambda}_2(t) = -\lambda_1(t) + \lambda_4(t)yb - \lambda_4(t)V\Gamma, & \lambda_2(t_f) = 0 \\ \dot{\lambda}_3(t) = \lambda_4(t)y\Gamma - \lambda_4(t)Vu_2, & \lambda_3(t_f) = 0 \\ \dot{\lambda}_4(t) = 0, & \lambda_4(t_f) = \lambda_0 \end{cases}$$

(1) If $t_2 = t_f$, $\lambda_1(t) = \lambda_2(t) = \lambda_3(t) = 0$ which contradicts $\lambda_3(t) = C\lambda_4(t)V(t)$ since $\lambda_4(t) \neq 0$ (otherwise $(\lambda_0, \lambda(t)) = 0$ violates the condition (1) of PMP) and $V \neq 0$ due to Remark 3.3. Thus there is no (t_1, t_f) on which $\Phi_2(t) = 0, \dot{\Phi}_2(t) = 0$, i.e u_2 is a bang-bang control on (t_1, t_f) for some t_1.

(2) If $t_2 < t_f$, observe that after substituting (3.5) into the adjoint equations in (3.2) in connection with the dynamics in (2.3), we have, for $t \in (t_1, t_2)$,

$$\begin{cases} \lambda_1(t) &= 2\lambda_4(t)by + \lambda_4(t)(u_1 - \frac{\Gamma^2}{C})x - \lambda_4(t)mF(t), \\ \dot{\lambda}_1(t) &= -\lambda_2(t)(\frac{\Gamma^2}{Cm} - \frac{u_1}{m}) = -\lambda_4(t)y(t)(\frac{\Gamma^2}{C} - u_1) \end{cases} \tag{3.6}$$

which has a solution if only $\dot{y}(t) = \frac{m}{2b}\dot{F}(t)$ since u_1 is a bang-bang control, see Proposition 3.4. Due to (3.5), (3.6), it is easy to check that

$$\ddot{\Phi}_2(t) =< \lambda(t), [R_d(X, u, t), [R_d(X, u, t), g_2(X)]] >= 0$$

and, on the other hand,

$$\begin{aligned}\Phi_2^{(3)}(t) =& < \lambda(t), [R_d(X,u,t), [R_d(X,u,t), [R_d(X,u,t), g_2(X)]]] > \\ &= \frac{2b\Gamma\lambda_4(t)V\left(C(by - F(t)m + \Gamma V + u_1 x) - \Gamma^2 x\right)}{C^2m^2} \\ &= -\frac{2b\Gamma\lambda_4(t)V}{Cm}\left(-\frac{1}{m}\left(u_1 - \frac{\Gamma^2}{C}\right)x - \frac{b}{m}y - \frac{V\Gamma}{m} + F(t)\right) \\ &= -\frac{2b\Gamma\lambda_4(t)V}{Cm}\dot{y} = -\frac{\Gamma\lambda_4(t)V}{C}\dot{F}(t)\end{aligned}$$

which cannot be identical to zero over any (t_1, t_2) and this is a contradiction to our assumption and therefore in this situation u_2 switches between $\underline{u_2}$, $\overline{u_2}$ on (t_1, t_2).

In conclusion, u_2 is always a bang-bang control. □

Taking into account two the preceding propositions, we obtain the following result.

Theorem 3.6. *Consider the optimization problem (2.3), the optimal controls u_1, u_2 are bang-bang.*

Proof. It is a combination of Proposition 3.4 and 3.5. □

4. Numerical Optimization and discussion

Observe that the system of ODEs in (2.3) is highly stiff due to the high drive frequency and needs to be approximated by suitable numerical methods with a sufficiently small time step size. Here, the numerical results are obtained with the help of the open-source software tool CasADi [19] with Python interface. The ODE system is discretized and solved by CVODES from the SUNDIALS integrator suite, see [20] and the obtaining nonlinear problem is solved by means of IPOPT [21]. For this particular problem, the time step is chosen to be smaller than 10^{-5} for the stability of the numerical solutions. The control problem is numerically challenging due to the different time scales that are involved. As a heuristic, we calculate a suboptimal solution by aggregating solutions on smaller time horizons $[t_i, t_{i+1}]$. We solve problem (2.3) on each sub-interval with the initial state $X(t_i)$ taken from the terminal state solution $X(t_i)$ of the preceding sub-interval and $X(t_0) = (0, 0, 0, 0)$, $t_0 = 0$. The aggregated trajectory $X(\cdot)$ on $[t_0, t_f]$ is not necessarily optimal, but provides an estimate for the possible improvement compared to state-of-the-art operation.

A simulation study can be implemented using the LT-Spice simulator with the device parameters adapted from [22] and listed in Table 1. Parameters of the linear two-port model are then [23]

$$C = \frac{C_0 + C_\mathrm{p} + C_\mathrm{L}}{2} \tag{4.1}$$

$$\Gamma = \frac{C_0 V_\mathrm{b}}{x_0} \tag{4.2}$$

$$K_1 = k_\mathrm{m} + \frac{2C_0^2 V_\mathrm{b}^2}{x_0^2\left(C_0 + C_\mathrm{p} + C_\mathrm{L}\right)} \tag{4.3}$$

TABLE 1. Example parameters for comb-drive capacitive transducers.

Parameters	**Value**
Proof mass, m	1.5 mg
Linear spring stiffness, k_{m}	3 N m^{-1}
Thin-film air damping, b	2.4e-5 Ns m^{-1}
Nominal capacitance, C_0	0.47 pF
Parasitic capacitance, C_{p}	7.5 pF
Load capacitance, C_{L}	8.6 pF
Nominal overlap, x_0	10 μm
Load resistance, R_{L}	16.9 MΩ
Bias voltage, V_{b}	24.9 V

The load resistance R_{L} and the open-circuit stiffness K_1 used in the lumped-model are kept fixed at optimal value of linear regime, adapted from [8], while the mechanical stiffness is a constant achieved from design. We are now considering the optimal problem in two cases: (i) there are no restrictions on proof mass motion and (ii) an identified constraint for displacement is taken into account.

4.1. **Power optimization for unconstrained displacement.** Here, we are considering the optimal performance of a harvester represented by mass-spring-damping system without any limit in mass motion. The displacement $x(t)$ therefore only depends on the external excitation level, drive frequency and damping constants [24].

4.1.1. *Acceleration sweep.* A sinusoidal acceleration sweep vibration input $F(t) = F_{\mathrm{a}}(t) = A_{\mathrm{r}} t g \cos(\omega t)$ is examined, where $t \in [t_0, t_{\mathrm{f}}] = [0, 1]$ s, $A_0 = 0$ g and $A_{\mathrm{f}} = 0.05$ g leading to $A_{\mathrm{r}} = 0.05$ g s^{-1}. The drive frequency is chosen as $\omega = \sqrt{\frac{K_1}{m}}$.

Figure 3 shows that the behaviors of the parameterized stiffness $\delta k = (K - m\omega^2)/\omega b$ and the electrical time constant $\omega\tau = \omega RC$ are identical to the theoretical analysis in Section 3, with $\delta k \in [0, 10]$ and $\omega\tau \in [\frac{1}{100}, 1]$. It is clear that the unexpected values of controls at some instance are due to numerical errors. The *bang-bang* characteristic of the optimal controls is still true for the following case. Figure 4 shows the improvement of the harvested power up to about 227% compared to an LT-Spice simulation.

4.1.2. *Frequency sweep.* In this case study, in stead of varying the acceleration amplitude, a linear swept-frequency cosine signal at the time instances $t \in [t_0, t_{\mathrm{f}}] = [0, 2]$ s is investigated, where $F(t) = F_{\mathrm{f}}(t) = A_{\mathrm{c}} g \cos(\omega_0 t + \frac{1}{2}\omega_{\mathrm{r}} t^2)$ with $A_{\mathrm{c}} = 0.05$ g, $\omega_0 = 200\pi$ rad s^{-1} and $\omega_{\mathrm{f}} = 800\pi$ rad s^{-1}. Thus, the swept rate of angular frequency is $\omega_{\mathrm{r}} = 300\pi$ rad s^{-2}. The numerical optimization of the output power is depicted in Figure 5 with more than 5 times higher than that of the simulated result.

4.2. **Power optimization under displacement-constraint operation.** In practical energy harvesters, the proof mass displacement must be restricted to avoid spring fracture

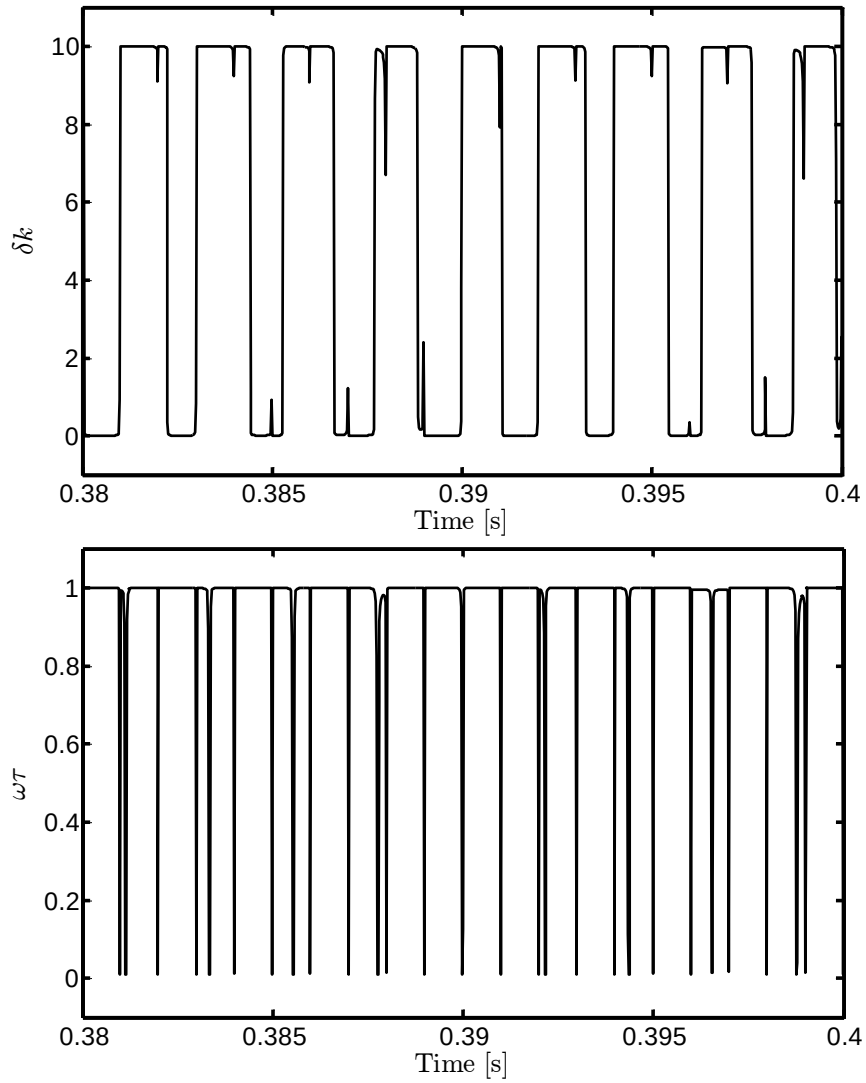

FIGURE 3. Closed-view waveforms of the parameterized stiffness and the parameterized load.

under high input acceleration amplitudes, or to be confined in finite dimensions of real structures. This can be implemented by design of the mechanical end-stops. In LT-Spice simulation, the impact mechanism during the contact period is modeled as Hertzian contact force, as shown in Figure 6. The impact force may then be written as a function of the relative displacement between the proof mass and the rigid end-stops $\delta = |x| - X_{\max}$ for $|x| \geq X_{\max}$, see [25]

$$F_{\text{im}} = k_{\text{im}}\delta^{\frac{3}{2}}\left(1 + \frac{3}{4}\frac{\dot{\delta}}{\dot{\delta}_{-}}\left(1 - e^2\right)\right) \tag{4.4}$$

where $X_{\max} = 5.5\ \mu m$, $k_{\text{im}} = 3.361$ MN m^{-1} is the impact stiffness, $\dot{\delta}_{-} = 8$ mm s^{-1} is the impact velocity and $e = 0.7$ is the coefficient of restitution. See [22] for detailed analysis.

Due to the special characteristics of the impact force [26, 27], numerical optimization problem (2.2), in which the second-order ODE is replaced by $m\ddot{x}(t) = -\left(K(t) - \frac{\Gamma^2}{C}\right)x(t) -$

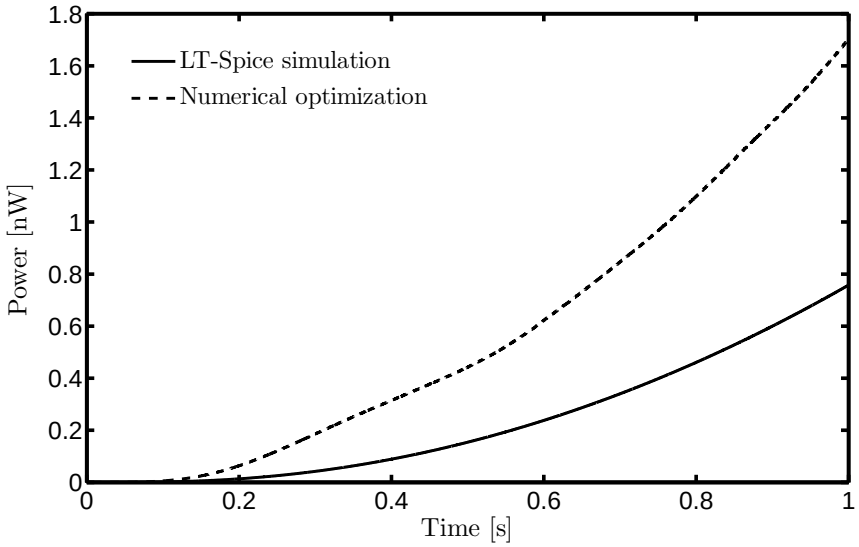

FIGURE 4. Numerical optimization result in comparison with simulation obtained from LT-Spice for the amplitude sweep of external acceleration.

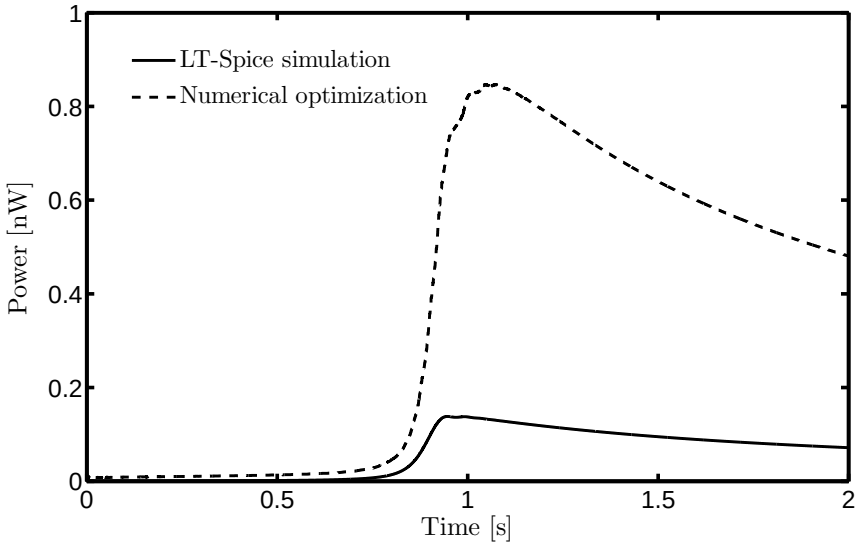

FIGURE 5. Numerical optimization result in comparison with simulation for the frequency-sweep excitation.

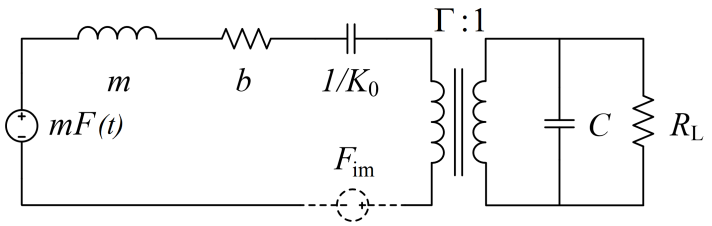

FIGURE 6. Two-port model in LT-Spice with impact force between the proof mass and the end-stops.

$b\dot{x}(t) - V(t)\Gamma + mF(t) - F_{\text{im}}$, is too challenging. Therefore, in this case, we consider the problem (2.2) affiliated with the condition $\frac{|x|}{X_{\max}} \leq 1$ instead.

Other parameters for acceleration sweep and frequency sweep forces are the same as in Section 4.1.

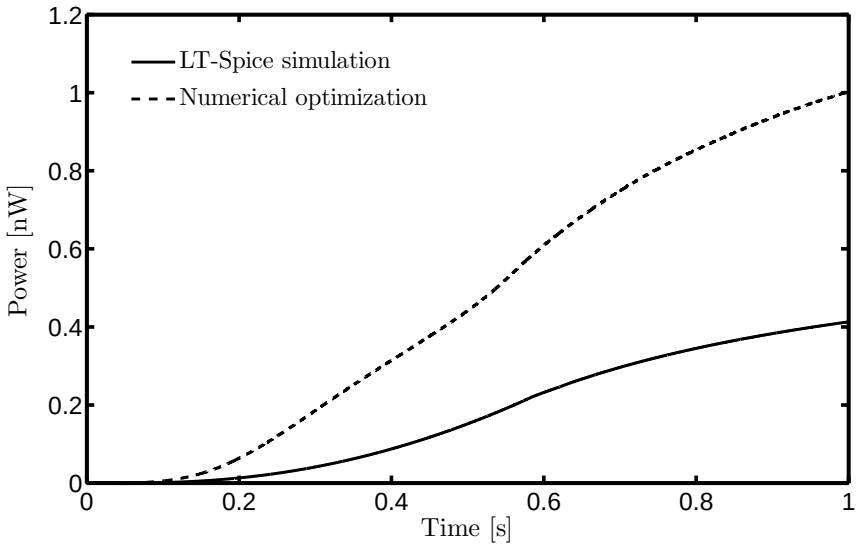

FIGURE 7. Numerical optimization results in comparison with simulation for the amplitude sweep of external acceleration, under displacement-constrained operation.

4.2.1. *Acceleration.* Figure 7 illustrates the numerical solution of optimum extracted power which is about 2.5 times higher comparing to the result achieved from simulation.

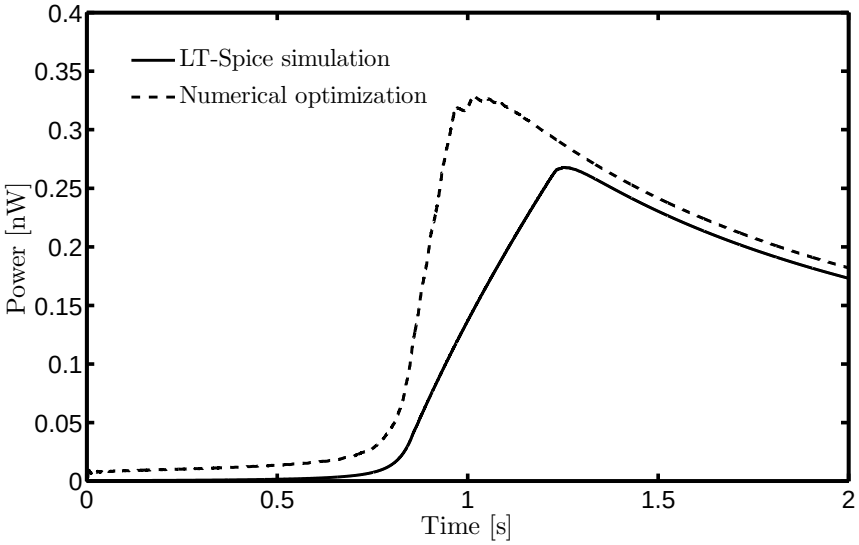

FIGURE 8. Numerical optimization and simulation results for the frequency-sweep excitation, with restriction of displacement.

4.2.2. *Frequency sweep.* Optimal value of the harvested power is solved numerically and presented in Figure 8. However, the improvement of output power is not much when t is in the range of $[1.25, 2]$ s. This can be explained by the difference between the behaviors of the

impact force in the lumped-model simulation and the mathematical condition $|x| \leq X_{\max}$ used for problem (2.2).

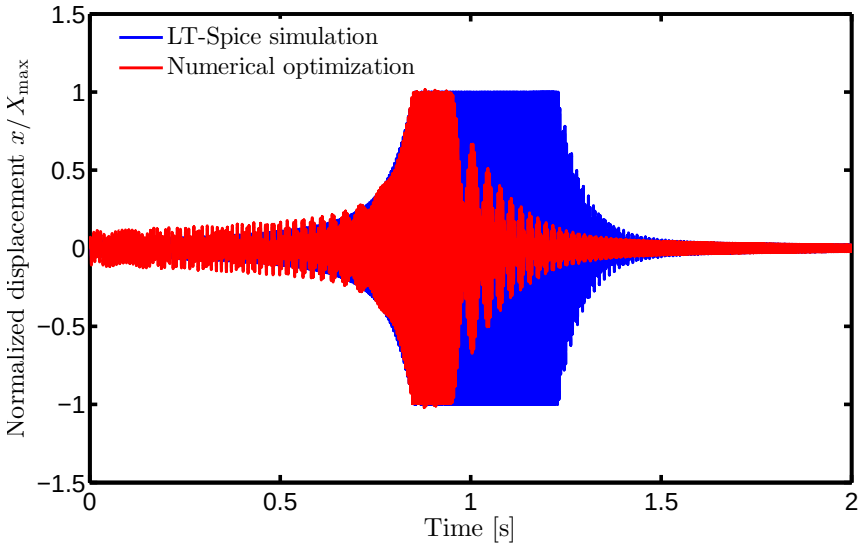

FIGURE 9. Comparison of the proof mass displacement in two case: (i) numerical optimization and (ii) simulation, for the frequency-sweep sinusoidal input.

MEMS energy harvesters exploiting impacts through alternative configurations were reported in [28–31], on both of modeling and experimental validations. These works exhibit the bandwidth enhancement in up-frequency sweep, i.e., going from low towards high frequencies. This phenomenon cannot be performed without Hertzian contact model or piecewise-linear restoring force, as in problem (2.2). Figure 9 shows the comparison of proof mass displacement as an evidence for the mentioned assertion.

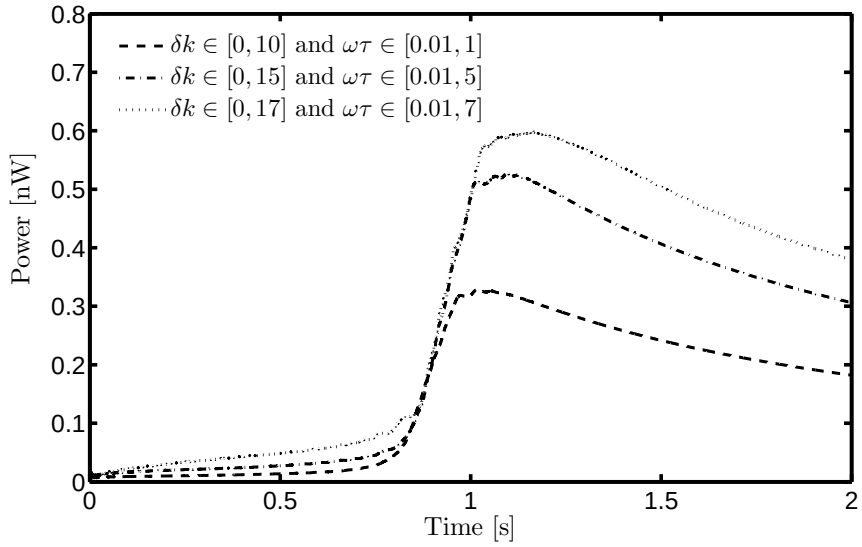

FIGURE 10. Comparison of the optimum output power with different ranges of the parameterized stiffness and the electrical time constant.

In summary, this work indicated the optimal behaviors of the two control subjects, load and stiffness, in order to maximize the extracted power of the vibration energy harvesters under unconstrained displacement. The numerical optimization results show significant enhancements of the transducer performances with different input forces and operating conditions. This is clearly an encouragement for future research on optimization on the whole time horizon. Owing to the bang-bang property, the resistive load and open-circuit stiffness now only need to be switched between upper and lower bounds which is of convenience for designing in practice, instead of being adjusted into each optimal one when the input driving force changes as analysis of previous work from other authors.

It is worth noting that the optimal output power here is only local value depending on setting of parameterized stiffness and electrical time constant bounds, see Figure 10 for an instance. The magnitude of these ranges can be appropriately chosen so that the global optimum value is achieved. Furthermore, an analysis of optimal behaviors of load and stiffness along with limitation of the mathematical model under displacement-constrained operation are also promising problems which need to be addressed.

Acknowledgment

Financial support from the European Research Council via the Consolidator Grant MODEST-647573 and the Research Council of Norway through Grant no. 4502084 are gratefully acknowledged. Thanks to Prof. Giovanni Colombo for his valuable suggestions.

References

[1] P. D. Mitcheson, E. M. Yeatman, G. K. Rao, A. S. Holmes, and T. C. Green, "Energy harvesting from human and machine motion for wireless electronic devices," *Proceedings of the IEEE*, vol. 96, pp. 1457–1486, Sept. 2008.

[2] S. Roundy, P. K. Wright, and J. Rabaey, "A study of low level vibrations as a power source for wireless sensor nodes," *Computer Communications*, vol. 26, pp. 1131–1144, July 2003.

[3] G. Ottman, H. Hofmann, A. Bhatt, and G. Lesieutre, "Adaptive piezoelectric energy harvesting circuit for wireless remote power supply," *IEEE Transactions on Power Electronics*, vol. 17, no. 5, pp. 669–676, 2002.

[4] J. M. Renno, M. F. Daqaq, and D. J. Inman, "On the optimal energy harvesting from a vibration source," *Journal of Sound and Vibration*, vol. In Press, Corrected Proof, pp. –, 2008.

[5] P. D. Mitcheson, T. C. Green, E. M. Yeatman, and A. S. Holmes, "Architectures for vibration-driven micropower generators," *Journal of Microelectromechanical Systems*, vol. 13, pp. 429–440, June 2004.

[6] E. Halvorsen, C. P. Le, P. D. Mitcheson, and E. M. Yeatman, "Architecture-independent power bound for vibration energy harvesters," *Journal of Physics: Conference Series*, vol. 476, no. 1, p. 012026, 2013.

[7] J. Heit and S. Roundy, "A framework to determine the upper bound on extractable power as a function of input vibration parameters," *Energy Harvesting and Systems*, vol. 3, no. 1, p. 069078, 2015.

[8] E. Halvorsen, "Optimal Load and Stiffness for Displacement-Constrained Vibration Energy Harvesters," *ArXiv e-prints*, Mar. 2016.

[9] C. Marboutin, Y. Suzuki, and N. Kasagi, "Vibration-driven MEMS energy harvester with vertical electrets," in *Proc. PowerMEMS 2007*, (Freiburg, Germany), pp. 141–144, 2007.

[10] H. Schättler and U. Ledzewicz, *Geometric optimal control: theory, methods and examples*, vol. 38. Springer Science & Business Media, 2012.

[11] A. Bressan and B. Piccoli, *Introduction to the mathematical theory of control*, vol. 2. American institute of mathematical sciences Springfield, 2007.

[12] U. Ledzewicz and H. Schättler, "Antiangiogenic therapy in cancer treatment as an optimal control problem," *SIAM Journal on Control and Optimization*, vol. 46, no. 3, pp. 1052–1079, 2007.

[13] A. d'Onofrio, U. Ledzewicz, H. Maurer, and H. Schättler, "On optimal delivery of combination therapy for tumors," *Mathematical Biosciences*, vol. 222, no. 1, pp. 13 – 26, 2009.

[14] U. Ledzewicz, M. S. F. Mosalman, and H. Schättler, "Optimal controls for a mathematical model of tumor-immune interactions under targeted chemotherapy with immune boost," *Discrete and Continuous Dynamical Systems - Series B*, vol. 18, no. 4, pp. 1031–1051, 2013.

[15] S. Sager, "Sampling decisions in optimum experimental design in the light of pontryagin's maximum principle," *SIAM Journal on Control and Optimization*, vol. 51, no. 4, pp. 3181–3207, 2013.

[16] E. Grigorieva and E. Khailov, "Optimal control of a nonlinear model of economic growth," *Discrete and Continuous Dynamical Systems*, pp. 456–466, 2007.

[17] E. V. Grigorieva and E. N. Khailov, "Hierarchical differential game between manufacturer, retailer, and bank," *Journal of Dynamical and Control Systems*, vol. 15, no. 3, pp. 359–391, 2009.

[18] H. A. C. Tilmans, "Equivalent circuit representation of electromechanical transducers: I. lumped-parameter systems," *Journal of Micromechanics and Microengineering*, vol. 6, pp. 157–176, 1996.

[19] J. Andersson, J. Åkesson, and M. Diehl, "Casadi: A symbolic package for automatic differentiation and optimal control," in *Recent Advances in Algorithmic Differentiation*, pp. 297–307, Springer, 2012.

[20] A. C. Hindmarsh, P. N. Brown, K. E. Grant, S. L. Lee, R. Serban, D. E. Shumaker, and C. S. Woodward, "Sundials: Suite of nonlinear and differential/algebraic equation solvers," *ACM Transactions on Mathematical Software (TOMS)*, vol. 31, no. 3, pp. 363–396, 2005.

[21] A. Wächter and L. T. Biegler, "On the implementation of an interior-point filter line-search algorithm for large-scale nonlinear programming," *Mathematical programming*, vol. 106, no. 1, pp. 25–57, 2006.

[22] B. D. Truong, C. P. Le, and E. Halvorsen, "Power optimization and effective stiffness for a vibration energy harvester with displacement constraints," *To appear*, 2016.

[23] C. P. Le and E. Halvorsen, "MEMS electrostatic energy harvesters with end-stop effects," *Journal of Micromechanics and Microengineering*, vol. 22, no. 7, pp. 74013–74024, 2012.

[24] C. B. Williams and R. B. Yates, "Analysis of a micro-electric generator for microsystems," *Sensors and Actuators A: Physical*, vol. 52, no. 1-3, pp. 8–11, 1996.

[25] H. M. Lankarani and P. E. Nikravesh, "Continuous contact force models for impact analysis in multibody systems," *Nonlinear Dynamics*, vol. 5, no. 2, pp. 193–207, 1994.

[26] V. Babitsky and V. Krupenin, *Vibration of Strongly Nonlinear Discontinuous Systems*. Engineering online library, Springer, 2001.

[27] L. I. Manevitch and O. V. Gendelman, "Oscillatory models of vibro-impact type for essentially non-linear systems," *Proceedings of the Institution of Mechanical Engineers, Part C: Journal of Mechanical Engineering Science*, vol. 222, no. 10, pp. 2007–2043, 2008.

[28] M. Soliman, E. Abdel-Rahman, E. El-Saadany, and R. Mansour, "A design procedure for wideband micropower generators," *Journal of Microelectromechanical Systems*, vol. 18, pp. 1288 –1299, dec. 2009.

[29] D. Hoffmann, B. Folkmer, and Y. Manoli, "Fabrication, characterization and modelling of electrostatic micro-generators," *Journal of Micromechanics and Microengineering*, vol. 19, no. 9, p. 094001 (11pp), 2009.

[30] H. Liu, C. J. Tay, C. Quan, T. Kobayashi, and C. Lee, "Piezoelectric mems energy harvester for low-frequency vibrations with wideband operation range and steadily increased output power," *Journal of Microelectromechanical Systems*, vol. 20, pp. 1131 –1142, oct. 2011.

[31] C. P. Le and E. Halvorsen, "An electrostatic energy harvester with end-stop effects," in *Proceedings of the 22nd Micromechanics and Microsystem Technology Europe Workshop*, (Tønsberg, Norway), June 19–22 2011.

(1) Institute of Mathematical Optimization, Mathematical Algorithmic Optimization, Otto-von-Guericke University, Magdeburg, 39106, Germany, Email: sager@ovgu.de

(2) Department of Micro- and Nano System Technology, University College of Southeast Norway, Email: Einar.Halvorsen@hbv.no